ACS APPLIED MATERIALS & INTERFACES

Research Article

www.acsami.org

Transparent Organosilica Photocatalysts Activated by Visible Light: Photophysical and Oxidative Properties at the Gas−Solid Interface

Emmanuel Arzoumanian,[†,⊥] Filippo Ronzani,[‡,⊥] Aurélien Trivella,[§] Esther Oliveros,[†] Mohamed Sarakha,[§] Claire Richard,[§] Sylvie Blanc,[‡] Thierry Pigot,[‡] and Sylvie Lacombe*[,‡]

[†]Laboratoire des IMRCP, UMR CNRS 5623, Université Toulouse III (Paul Sabatier, UPS), 118 route de Narbonne F-31062 Toulouse Cedex 9, France

[‡]IPREM, UMR CNRS 5254, Université de Pau et des Pays de l'Adour, Hélioparc, 2 rue du Président Angot, F-64053 Pau Cedex 9, France

[§]ICCF, UMR CNRS 6296, Université Blaise Pascal, Campus des Cézeaux, 24 avenue des Landais BP 80026, F-63171 Aubière Cedex, France

Supporting Information

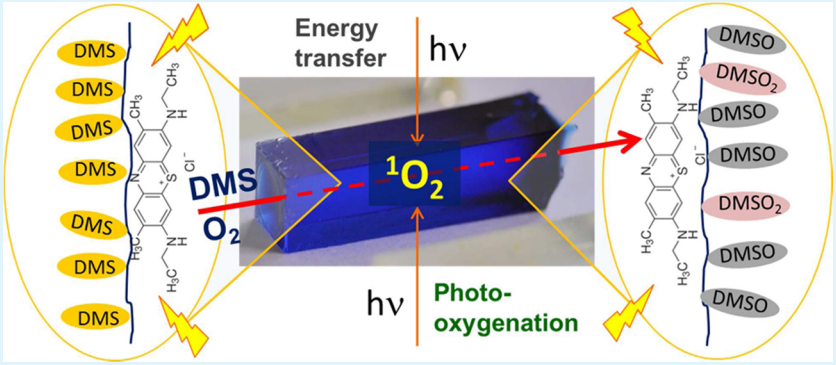

ABSTRACT: The photophysical properties of several photosensitizers (PSs) included or grafted in silica monoliths were compared to their properties in solution. The effects of the solid support on their steady-state and transient absorption spectra, on their quantum yields of singlet oxygen ($^1O_2$) production, and on their ability to photoinduce the oxidation of dimethylsulfide (DMS) were investigated. Two cyanoanthracene derivatives (9,14-dicyanobenzo[*b*]triphenylene, **DBTP**, and 9,10-dicyanoanthracene, **DCA**), as well as three phenothiazine dyes (methylene blue, **MB**$^+$, new methylene blue, **NMB**$^+$, methylene violet, **MV**), were encapsulated in silica, analyzed and compared to two reference PSs (perinaphthenone, **PN** and rose bengal, **RB**). A **DBTP** derivative (3-[*N*-(*N*″-triethoxysilylpropyl-*N*′-hexylurea)]carboxamido-9,14-dicyanobenzo[*b*]triphenylene, **3**) was also prepared and grafted onto silica. Thanks to the transparency and the free-standing shape of the monoliths, the complete spectroscopic characterization of the supported PSs was carried out directly at the gas−solid interface. The influence of the silica network, the PS, and the adsorption/grafting link between the PS and silica was investigated. The effects of PS concentration, gaseous atmosphere, humidity, and hydrophobicity on the production of $^1O_2$ were analyzed. With all PSs, $^1O_2$ production was very efficient (quantum yields of $^1O_2$ production, relative to **PN**, between 0.6 and 1), and this species was the only one involved in the pollutant photooxidation. The influence of the matrix on the PSs' photophysics could be considered as negligible. In contrast, the matrix effect on DMS photooxidation was extremely important: the gas diffusion inside the porous structure, and thus, the photoactivity of the materials, strictly depended on silica's surface area and porosity. Our results highlight the suitability of these silica structures as inert supports for the study of the photosensitizing properties at the gas−solid interface. Moreover, thanks to the adsorption properties of the matrix, the synthesized materials can be used as microphotoreactor for the $^1O_2$-mediated oxidation of volatile pollutants.

KEYWORDS: *silica, porous material, singlet oxygen, photosensitizer, transient species, photooxidation*

INTRODUCTION

Photosensitization is one of the most convenient routes for singlet oxygen ($^1O_2$) generation due to the mild conditions of the process: visible-light irradiation, room temperature, and molecular oxygen as the only reagent.[1] Singlet oxygen applications cover many fields of chemistry: water and air decontamination/detoxification[2,3] and photocatalytic oxygenations in solar and green chemistry,[4,5] as well as biomedical aspects such as disinfection and photodynamic therapy (PDT).[6−9] Many organic photosensitizers (PSs) are already known and used to generate $^1O_2$ in homogeneous solutions.[1,10] Nonetheless, it is more convenient to design photoactive materials, where photosensitizers are bound to inert supports. Several supports and grafting methods have already been

Received: September 24, 2013
Accepted: December 4, 2013
Published: December 4, 2013

developed and have found widespread applications.[11−15] The interaction of the PS with the supporting matrix may influence its photophysical properties. However, if extensive analysis of the PS photophysics in such highly scattering media is possible,[16,17] the monitoring of their transient is more scarce.[18,19] Quantum yields of $^1O_2$ production may be determined *in suspensions*, as previously published for methylene blue supported on Nafion[19] or porous silicon,[20] protoporphyrin in silica spheres,[21] porphyrins intercalated in layered double hydroxides,[22] or phthalocyanines and pyrylium salts in zeolites.[23]

We have recently shown that PSs can be inserted in transparent highly porous silica monoliths or films which can be used as solvent-free microreactors for photochemical applications at the gas−solid interface.[24−28] These bulk materials present many advantages: transparency optimizes light harvesting by the PS,[29,30] high porosity and specific surface area give these matrices efficient adsorption properties (for both the reactants and the products),[31] sol−gel syntheses are easily carried out, silica is inert and easily modified during the preparation steps,[32−35] and many PSs can be grafted on functionalized materials.[36] As already demonstrated, silica monoliths doped with cyanoanthracene derivatives can efficiently produce singlet oxygen[25] and oxidize sulfides at the gas−solid interface.[24−26,37]

The aim of the present work was to investigate the ground and excited state properties of several PSs included or grafted in silica monoliths, in comparison with their properties in solution, by investigating the effects of the solid support on their absorption/emission and their transient spectra, on their quantum yields of singlet oxygen production (Φ_Δ) and on their ability to photoinduce the oxidation of gaseous dimethylsulfide (DMS).[38,39] Thanks to silica transparency and to the monoliths free-standing shape, the complete spectroscopic characterization of the silica-embedded PSs was carried out directly at the gas−solid interface without any suspension in a solvent. The influence of the silica network, the nature of the dye, and the adsorption/grafting link between the PS and silica were investigated. In addition to **DCA** (9,10-dicyanoanthracene), **DBTP** (benzo[*b*]-triphenylene-9,14-dicarbonitrile), and one of its graftable derivatives (3-[*N*-(*N*″-triethoxysilylpropyl-*N*′-hexylurea)]-carboxamido-9,14-dicyanobenzo[*b*]triphenylene **3**),[40] various dyes were chosen either as reference PSs in the visible (rose bengal **RB**,[41] methylene blue **MB**$^+$[42]) and in the UV (perinaphtenone **PN**[43]) or because of their extensive use in biology despite the paucity of the reported photophysical data (new methylene blue **NMB**$^+$,[44] methylene violet **MV**,[44−46] Scheme 1). The effects of the solid support on the stationary absorption/emission and transient absorption were investigated, and $^1O_2$ production in the prepared materials was detected and quantified under various conditions. The effects of PS concentration, gaseous atmosphere, humidity and hydrophobicity of the matrix were analyzed. The activities of the supported PSs in the photosensitized oxidation of DMS were also compared.

EXPERIMENTAL SECTION

The chemicals used and the synthetic procedures for the preparation of **2** and **3** are described in the Supporting Information (SI), section S01.

Synthesis of Silica Monoliths. Transparent silica monoliths were obtained by the conventional hydrolysis and condensation of TMOS in the presence of MeOH and water (sol−gel method).[24] A 1/5/4:alkoxide/alcohol/water molar ratio was chosen. The TMOS + MeOH + PS mixtures were first stirred two minutes at room temperature. After the addition of water, the sols were stirred for 2 min more. For the gelation step, the sols were then poured into disposable UV-cuvettes (3.5 mL each) which were stored firmly closed for 3 weeks at 55 °C (gelation).

Scheme 1. Chemical Structure of the Studied PSs[a]

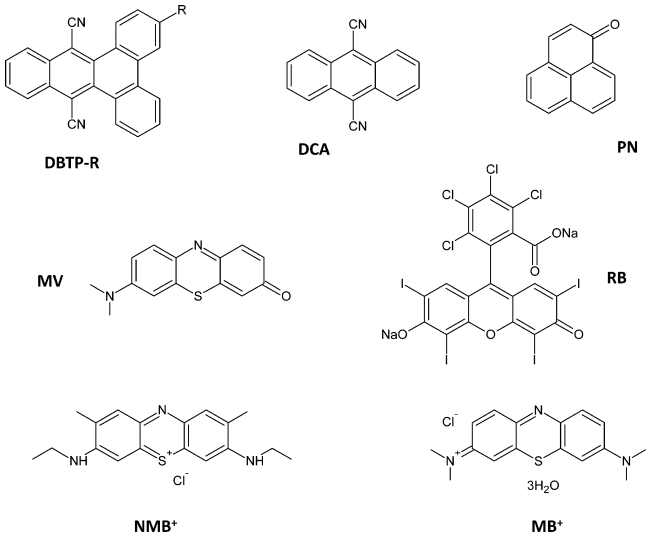

[a]For **DBTP**-derivatives, **DBTP**: R = H. **1**: R = CO−NH−$(CH_2)_6$−NH−Boc. **2**: R = CO−NH−$(CH_2)_6$−NH_2. **3**: R = CO−NH−$(CH_2)_6$−NH−CO−NH−$(CH_2)_3$−Si−$(OEt)_3$.

Afterward, the cuvettes were opened and stored 4 weeks at 30 °C (aging). Finally, the temperature was raised to 50 °C for 2 days (drying). The detailed ratios of each component for the various monoliths are listed in Table 1.

Table 1. Volumes of Solvents, Water, and Silica Precursors Added for the Synthesis of the Different Types of Monoliths

monolith	vol MeOH/mL	vol ACN/mL	vol H_2O/mL	vol TMOS/mL	vol TMOS-OC/mL
SG0	1.677		0.598	1.225	
SG0-ACN	0.784	1.012	0.559	1.145	
SG0-OC 2%	1.669		0.595	1.218	0.042
SG0-OC 5%	1.656		0.590	1.209	0.105
SG2-ACN	1.677	1.012	0.598	1.225	

PSs were usually encapsulated in the silica matrix (**SG0**). For all the **SG0** syntheses, solutions of the photosensitizers in MeOH were prepared and suitable volumes were added to the starting sols (TMOS + MeOH): volumes were calculated in order to maintain the established molar ratio and to obtain monoliths at different PSs concentrations and absorbances (see Tables 2, 6, and 7).[24]

In case of monoliths bearing octyl groups (**SG0-OC**), small volumes of TMOS-OC (TMOS/TMOS-OC/MeOH/H_2O = 1−*x*/*x*/5/4, where *x* = 0.02−0.05) were added to the starting sols.

Some monoliths with TMOS as the only alkoxide were prepared with a MeOH/ACN[47] mixture as solvent (TMOS/MeOH/ACN/H_2O = 1/2.5/2.5/4, **SG0-ACN**).

To graft **DBTP** onto silica (**SG2-ACN**), the PS-silyl derivative **3** was introduced directly in the sol in a mixture of MeOH and ACN (molar ratio 1/1), since the synthesis of **3** was carried out in ACN, together with TMOS as main alkoxide (same molar ratio as for **SG0**). Different volumes of the freshly prepared solution containing **3** were added during the first phase of the sol−gel synthesis.

Materials and Methods. Nitrogen adsorption and desorption isotherms of the silica monoliths were measured at 77 K on a Micromeritics ASAP 2010 Micropore nitrogen adsorption apparatus. UV−vis spectra were obtained on a Varian Cary 5E UV−vis-NIR spectrophotometer in steps of 0.5 nm using a homemade sample holder. The diffuse reflectance UV−vis spectra (DRUV) were measured in steps of 1 nm with a Perkin-Elmer 860 Spectrophotometer equipped with a 15 cm diameter-integrating sphere bearing the holder in the bottom horizontal position. The instrument was calibrated with a certified

Table 2. PSs Concentrations in the Starting Sols and in the Final Monoliths[a]

	$[PS]_{sol}/10^{-6}$ M		$[PS]_{mon}/10^{-8}$ mol g^{-1}	
PS	min	max	min	max
DBTP	5.7[b]	14.0[b]	4.0[b]	9.8[b]
	9.1[c]	34.3[c]	6.4[c]	24[c]
DCA	10.0	25.1	7.0	17.6
PN	8.0	16.3	5.6	11.4
		(>7.7×10^{-5})[d]		(>5.4×10^{-7})[d]
RB	0.7	1.5	0.5	1.0
MB^+	10.6	37.1	7.4	26.0
NMB^+	9.7	18.0	6.8	12.6
MV	8.3	16.0	5.8	11.2

[a]Data corresponding to the materials used for spectroscopic studies (for photooxidation tests see Tables 6 and 7). Uncertainty: approx 10%. [b]Relative to all **SG0-DBTP** monoliths, including **SG0-OC** and **SG0-ACN**. [c]Relative to **SG2-ACN** monoliths (compound **3** as **DBTP** derivative). [d]Concentration corresponding to absorbance saturation (see singlet oxygen detection). Minimum concentration since actual determination of the concentration was not possible due to an absorbance ≥2 in the monolith (see singlet oxygen detection).

Spectralon white standard (Labsphere, North Sutton, USA). Corrected steady-state emission and excitation spectra were measured using a photon counting Edinburgh FLS920 fluorescence spectrometer equipped with a Xe lamp. Time-resolved fluorescence experiments were carried out by using a nanosecond flash lamp (nF900) and time-correlating single photon counting (TCSPC). The lifetime data were analyzed with the reconvolution fit (including instrument response) of the Edinburgh software.

For the detection of transient species a Nd:YAG laser (GCR 130−1, pulse width 9 ns, 355 nm) was used for the samples irradiation. The monitoring system consisted of a 150 W pulsed xenon arc lamp, a R928 photomultiplier and a 05-109 Spectra Kinetics Applied Photophysics monochromator. Signals were digitized by a HP54522A oscilloscope. The samples were irradiated in a homemade Teflon sample holder. The laser pulse energy (P) was measured using a joulemeter Ophir Optronics Ltd.

Singlet oxygen was detected by its weak phosphorescence emission centered at approximately 1270 nm, under both continuous (SSPD) and time-resolved (TRPD) excitation of the PS.[48−55] A complete description of the two experimental procedures and set-ups for $^1O_2$ detection is reported in section SI02, SI.

The solid−gas photooxidation (PO) of dimethylsulfide (DMS) was performed in a pass-through reactor[56,57] (procedure and setup detailed in section SI03 and Figure SI 1, SI). After DMS adsorption in the dark, two irradiation−resaturation cycles followed (24 h irradiation periods). Lamps (Figure SI 2, SI) with emission maxima at 420 and 575 nm were used to irradiate **DBTP/DCA/PN** and **NMB^+/MB^+/MV/RB** based materials, respectively. The gas outlet was analyzed by GC-FID. The photooxidation activity was evaluated in terms of conversion percentage normalized by the photon flux absorbed by the PS. The reaction products were desorbed and analyzed by GC-MS. DRUV spectra were recorded before and after the photooxidation tests to estimate the bleaching of the PSs upon irradiation.

RESULTS AND DISCUSSION

Syntheses and Structural Characterization. Compound **2** was prepared following usual conditions for Boc-deprotection reactions (Scheme 2).[58] The addition of trifluoroacetic acid broke the carbamate linker, forming an ammonium salt between the amino-derivative of **DBTP** and TFA, further neutralized by the addition of KOH. The reaction was easily followed by TLC, but the poor solubility of **2** made any NMR characterization impossible. Compound **3** (Scheme 2) was obtained by a one-pot condensation of TEOS-NCO (3-(triethoxysilyl)propylisocyanate)

Scheme 2. Synthesis of Compounds 2 and 3 from 1

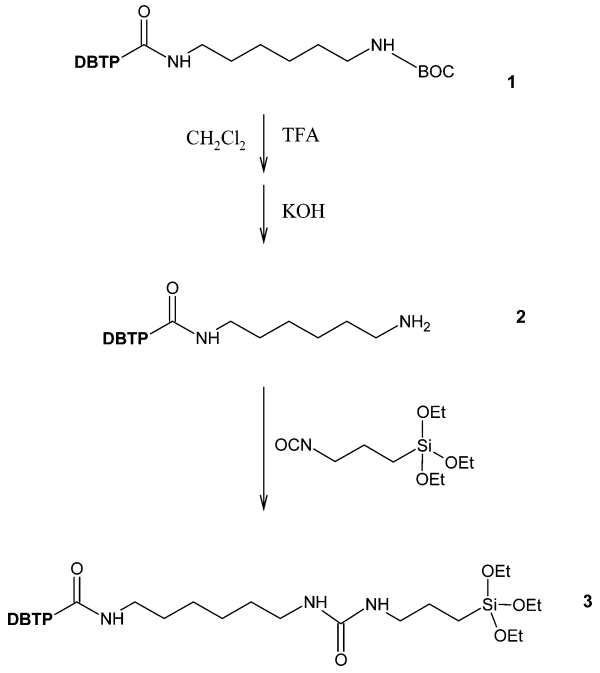

with the amino moiety of **2** under strictly anhydrous conditions to avoid polycondensation reactions of the triethoxysilyl-derivative. The reaction between primary amines and isocyanates is very fast and efficient and leaves no byproduct: completion was reached after some hours under stirring at room temperature. The freshly prepared ACN solution containing **3** was then directly added to the MeOH solution for monoliths synthesis.

Several kinds of highly transparent silica monoliths were prepared and characterized by their specific surface area and porosity:

- **SG0** for included PSs (no grafting) using only TMOS and solutions of PSs in methanol,
- **SG0-ACN** when a mixture methanol-acetonitrile (50/50 molar) was used as the solvent,
- **SG0-OC** when mixtures TMOS/TMOS-OC (2−5% molar in trimethoxy(octyl)-silane (TMOS-OC)) were used to obtain more hydrophobic silica,
- **SG2-ACN** when **3**, dissolved in an ACN/MeOH mixture (50/50 molar), was used together with TMOS. In this case the silyl derivative **3** participates to the polycondensation process and the PS is consequently grafted to the matrix.

Silica monoliths were characterized by N_2 adsorption−desorption isotherms (Table 3). All the monoliths presented a very high specific surface area (>555 m^2 g^{-1}) and were mainly microporous, but with a non-negligible percentage of mesopores (22−38% of the total surface area). Optical transparency and uniform distribution of the PSs were usually observed in **SG0** monoliths (Figure 1). Nonetheless, for **SG0-RB** more intensely colored layers appeared at the top of the monoliths: owing to a lower affinity to silica, **RB** probably followed the solvent during its evaporation, resulting in a higher concentration at the top of the xerogel. Approx 20% of the weight of the materials was due to adsorbed water (Table 3), which could be eliminated after 4 to 5 h treatment under primary vacuum at 80 °C. To decrease the hydrophilic character of **SG0** monoliths,[32,59,60] different amounts of TMOS-OC (2 → 5%, **SG0-OC**)[61] were added to the initial sols. The octyl substituent accelerates the rate of hydrolysis by

dx.doi.org/10.1021/am404175y | ACS Appl. Mater. Interfaces 2014, 6, 275−288

Table 3. Structural Analysis of Silica Monoliths[a]

monolith	S_{BET}/m^2 g^{-1}	% mesopores[b]	A_{pores}/m^2 g^{-1}	V_{pores}/cm^3 g^{-1}	$Ø_{pores}$/Å	H_20/%
SG0	605	22 ± 3	135	0.108	34	18
SG0-OC 2%	640	23 ± 3	146	0.103	29	12
SG0-OC 5%	555	23 ± 3	131	0.140	47	13 (11)
SG0-ACN-DBTP	730	30 ± 4	222	0.176	33	16 (20)
SG2-ACN-DBTP	660	38 ± 5	252	0.228	37	15 (18)

[a]Surface area (BET method, relative uncertainty = 10%), relative percentage, area, volume, and diameter of mesopores (BJH method, relative uncertainty = 10%), water percentage measured by sample weighting before and after drying under vacuum at 80 °C and, in brackets, by TG-MS analysis. [b]Estimated by the ratio between A_{pores} and S_{BET}.

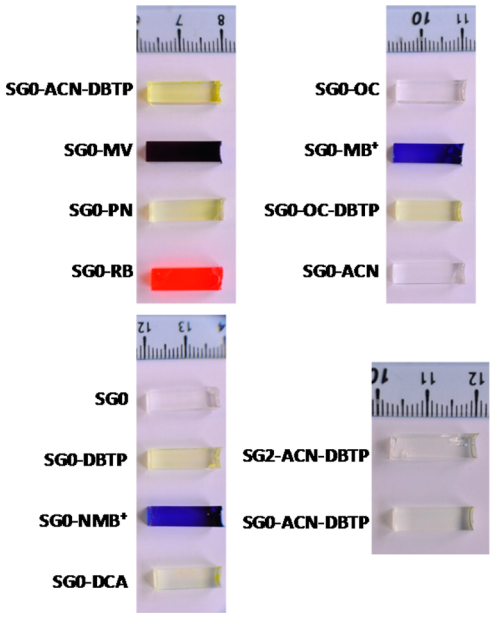

Figure 1. Some silica monoliths. (left) **SG0-ACN-DBTP**, **SG0-MV**, **SG0-PN**, **SG0-RB**, **SG0**, **SG0-DBTP**, **SG0-NMB$^+$**, **SG0-DCA**. (right) **SG0-OC** 2.5% OC, **SGO-MB$^+$**, **SG0-OC-DBTP** 1% OC, **SG0-ACN**, comparison between **SG2-ACN-DBTP** and **SG0-ACN-DBTP**.

stabilizing the positive charge formed on the Si atom. As expected, in the final **SG0-OC**, adsorbed water (Table 3) decreased from 20% to approximately 12% of the total mass. Their specific surface area was maintained over 555 m^2 g^{-1} without any significant influence on the microporous/mesoporous ratio. The 50/50 molar mixture of MeOH and ACN was used to increase the PS amount in **SG0-DBTP** monoliths (**DBTP** is more soluble in the mixture of the two solvents) and to better compare encapsulated (**SG0-ACN**) and grafted (**SG2-ACN**) **DBTP**. The use of ACN as a cosolvent was not expected to significantly influence the reaction parameters: the structure of **SG0** and **SG0-ACN** monoliths was macroscopically similar, even though the addition of ACN made the specific surface area and the mesoporosity increase from 605 to 730 m^2 g^{-1} and from 22 to 30%, respectively. In addition, since MeOH and ACN have similar relative static permittivity (ε_r),[62] the migration of the PS during the synthesis and its final distribution inside the monolith did not strongly vary using MeOH or MeOH + ACN.

SG2-ACN-DBTP monoliths were prepared using freshly prepared **3** as starting material. The one-pot condensation between the amine group of **2** and the silyl-isocyanate was chosen to prevent the formation of byproducts[40,63−66] and to avoid postgrafting steps which could endanger the structural stability of the material. A strict stoichiometry control was necessary to avoid the presence of free NCO functions in the sol: while usually disfavored, NCO hydrolysis can occur under the sol−gel conditions (high temperature, high water concentration) and prevent the formation of a transparent and compact structure. **SG2-ACN-DBTP** monoliths were transparent and macroscopically similar to their **SG0** counterparts, with high mesoporous character (38%) and specific surface area (660 m^2 g^{-1}), though slightly more fragile: it is thus possible to graft **DBTP**-derivatives to silica without the formation of any byproduct and without jeopardizing the optical and structural properties of the monoliths.

Spectroscopic Characterization. *UV−vis Absorption and Fluorescence Spectroscopy.* The transparent silica monoliths could be analyzed by transmission UV−vis spectroscopy since silica absorption was strictly limited to the UV (λ < 300 nm, dotted line in Figure 2); DRUV−vis spectra could also be recorded (Figure SI 3, SI). Except for too concentrated **SG0-MB$^+$** and nonfluorescent **SG0-PN**, fluorescence excitation and emission spectra were recorded for all the samples (Figure 3 and Figures SI 4−6, SI). In most cases, the influence of the silica matrix (**SG0**) on the position of the absorption bands and on the molar absorption coefficients appeared negligible (relative to polar solvents).[40,44,67−69] Only for **MV**, which is very sensitive to the environment,[45,69] the effect of silica was more significant since the maximum fluorescence wavelength shifted by 28 nm to the red relative to methanol, in agreement with an increase of the polarity of the medium.[45] The emission properties of **DBTP** monoliths (Figure 3) deserve special comments. In polar solvents, **DBTP** forms a complex in the excited state:[67] this species emits at longer wavelength (500 nm in MeOH, unstructured signal) relative to the monomer (420 nm in hexane). Moreover, considering functionalized **DBTP** in a given solvent, a bathochromic shift, inversely proportional to the polarity of the substituent, is observed.[40] Since **DBTP** is less polar than its derivative **3**, the bathochromic shift of its emission maximum in **SG0-ACN-DBTP** relative to **SG2-ACN-DBTP** (by approximately 30 nm, Table 4) is more related to the substituent than to silica.

For the three phenothiazine derivatives (**MB$^+$**, **NMB$^+$**, and **MV**), very short fluorescence lifetimes were measured, in contrast to **DBTP** and **DCA** (Table 4). For **SG0-MB$^+$**, the biexponential decay (0.6 and 1.4 ns) was consistent with our recently published data[69] and with previous results from Dunn et al.[70] in water (0.37 (91%) and 0.82 (9%) ns) and from Wetzler et al.[19] for Nafion-supported **MB$^+$** (0.2 (89%) and 1.7 (11%) ns). **MV** and **NMB$^+$** fluorescence decayed monoexponentially with lifetimes close to 1 ns, similar to τ_F in solutions.[45,69] Two fluorescence lifetimes were also obtained with **DCA**- and **DBTP**- monoliths. For **SG0-DCA**, the two lifetimes (12.2 and 5.6 ns) are reminiscent of the values obtained respectively in air-equilibrated (12.7 ns) and in oxygen-saturated (7.6 ns) ACN solutions,[67] as if the main fraction of **DCA** was forced in the pores together with higher concentrations of singlet excited state

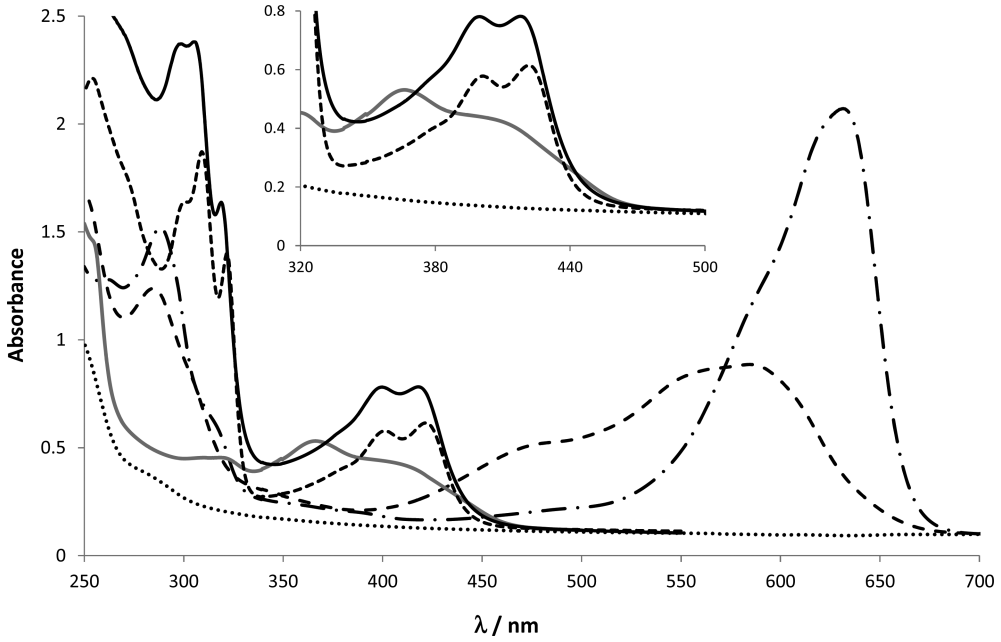

Figure 2. Transmission UV−vis spectra of some PSs in silica monoliths. **SG0-NMB**$^+$ (dashed-dotted line), **SG0-MV** (long-dashed line), **SG0-ACN-DBTP** (black solid line), **SG0-OC-DBTP** (dashed line), **SG0-PN** (gray solid line) and blank silica sample (dotted line). (inset) Detailed region between 330 and 500 nm.

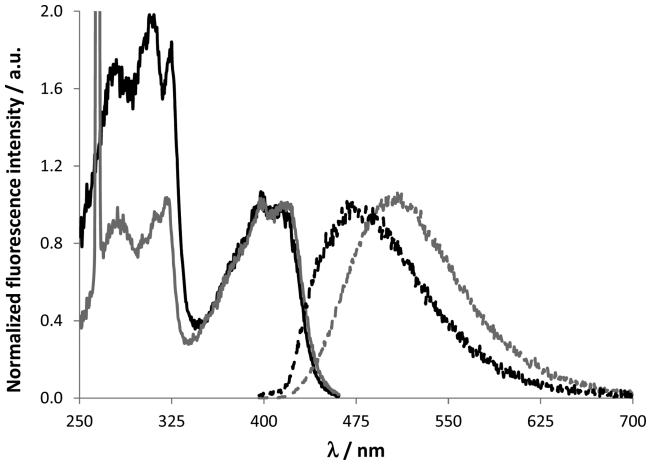

Figure 3. Fluorescence excitation (λ_{em} = 470 nm) and emission (λ_{ex} = 385 nm) spectra of **DBTP**-derived silica materials: **SG0-ACN-DBTP** (gray) and **SG2-ACN-DBTP** (black).

quenchers (mainly oxygen). Similarly, for **SG0-ACN-DBTP** and **SG2-ACN-DBTP** monoliths (2.1 and 7.2 ns, and 1.9 and 8.0 ns, respectively), a good agreement was found between the lifetimes of the main shortest-lived components and the values in oxygenated solutions (1.3 and 3.2 ns in chloroform and methanol, respectively), while the longest-lived component shows lifetime values closer to those in air-equilibrated solutions (between 2.4 and 5.4 ns).[67]

Analysis of the Transient Species. The transient species generated by excitation of the PSs were studied directly inside the monoliths by means of nanosecond laser flash photolysis. Absorption spectra (Figures 4 and 5) and lifetimes (Table 4) were measured. Ground state photobleaching prevented the exact determination of the absorption maxima for all the PSs. The linear dependence of the transient absorbance on both the laser pulse energy (5−28 mJ) and the PS concentration ($\approx 10^{-7}$ mol g^{-1}) confirmed the monophotonic formation of the transient species and the absence of dimeric species (aggregation) in the ground state.

The transient absorption spectra recorded for **SG0-PN** (three apparent maxima at 340, 400, and 490 nm, Figure 4a) and **SG0-DCA** (maximum between 390 and 470 nm, Figure 4b), were consistent with those reported in the literature and assigned to triplet−triplet absorption. It is interesting to notice that the triplet absorption spectrum of **DCA** is more easily observed in the monolith than in solution, where heavy atoms are usually added to enhance intersystem crossing.[71−73] The transient absorption spectra of **DBTP**, in both **SG0** and **SG0-ACN** materials, were very similar to those obtained in ACN solutions:[40] the two apparent maxima at approximately 370 and 470 nm (Figure 4c) were exclusively assigned to the triplet excited state. The triplet spectra and decay were similar for **SG0** and **SG0-ACN** matrices (Figure SI 8, SI) showing that there is no difference in the photophysical properties of **DBTP** in these two media.

The transient absorption spectrum of **SG0-RB** (Figure SI 7, SI) showed apparent maxima at 370, 590, and 680 nm. This spectrum was poorly consistent with the already scattered literature data: Murasecco-Suardi et al.[74] reported an absorption maximum at 470 nm, Grajcar et al.[75] at 820 nm, Ketsle et al.[76] reported two maxima at 450 and 620 nm, and Shimizu et al.[77] observed an absorption maximum at 1070 nm. This was probably due to the nonhomogeneous **RB** distribution inside silica.

For **SG0-MB**$^+$ (Figure SI 7, SI) the two maxima at 370 and 420 nm were assigned to the triplet excited state. The triplet−triplet absorption is probably superimposed with that of the radical dication. In acetonitrile, the transient absorption spectrum of **MB**$^+$ is characterized by a band at 420 nm assigned to the triplet excited state and by a less intense band at 520 nm, assigned to prompt formation of the radical dication. To our knowledge, no transient species has been reported to absorb around 370 nm for **MB**$^+$. Hence, the T−T absorption spectrum recorded for **SG0-MB**$^+$ seems to be significantly blue-shifted (approximately 50 nm) relative to that recorded in ACN or MeOH (430 nm).[78,79] The matrix effect is thus very important.

The transient absorption spectra of **SG0-MV** (Figure 5a) and **SG0-NMB**$^+$ (Figure 5b) were close to the one obtained

Table 4. Spectroscopic Characterization of PS-Doped SG Materials[a]

monolith	λ_{max}/nm ($\lambda_{max,MeOH}$)	$\varepsilon_{\lambda,max}$/M^{-1} cm^{-1} [c] ($\varepsilon_{\lambda,max,\ MeOH}$)	$\lambda_{max,em}$/nm ($\lambda_{max,MeOH}$)	τ_F/ns (*solution*)	τ_T/μs (λ_{max}/*nm*)	$k_{d,T}$/10^5 s^{-1}
SG0-RB	550 (*555*)	43 000 (*85000*)	563 (*570*)			
SG0-MB$^+$	650 (*655*)	– (*72000*)		τ_1 0.6 (90%) τ_2 1.4 (10%) (*0.6 MeOH, air*) (*1.0 ACN, air*)	4.5 ± 0.1 (*420 nm*)	2.2 ± 0.2
SG0-NMB$^+$	635 (*628*)	60000 (*73000*)	644 (*649*)	τ_1 0.7 (*0.7 MeOH, air*) (*0.8 ACN, air*)	3.8 ± 0.1 (*420 nm*)	2.6 ± 0.3
SG0-MV	592 (*603*)	39900 (*21600*)	666 (*638*)	τ_1 0.9 (*0.5 MeOH, air*) (*1.5 ACN, air*)	4.8 ± 0.2 (*365 nm*)	2.1 ± 0.2
SG0-PN[b]	370 (*363*)	9600 (*10200*)			3.4 ± 0.1 (*490 nm*)	2.9 ± 0.3
SG0-DCA	426 (*423*)	7000 (*10800*)	434 (*436*)	τ_1 5.6 (74%) τ_2 12.2 (26%) (*12.7 ACN, air*) (*7.6 ACN, O_2*)	2.0 ± 0.1 (470 nm)	5.1 ± 0.5
SG0-DBTP	420 (*415*)	5000 (*9500*)	508 (*493*)		0.3 ± 0.05 (*470 nm*)	35 ± 3
SG0-OC−DBTP 2% OC	425 (*415*)	7 550	502 (*493*)			
SG0-ACN-DBTP	421 (*415*)	5 600	500 (*493*)	τ_1 2.1 (79%) τ_2 7.2 (21%) (*5.4 MeOH, air*) (*3.2 MeOH, O_2*)	0.3 ± 0.05 (*470 nm*)	31 ± 4
SG2-ACN-DBTP	424[d] (*415*)	4500[d]	470 (*493*)	τ_1 1.9 (78%) τ_2 8.0 (22%) (*5.4 MeOH, air*) (*3.2 MeOH, O_2*)		

[a]Maximum absorption wavelengths for the 0−0 transition (in brackets the corresponding value for PSs in MeOH), molar absorption coefficients at λ_{max}, maximum wavelengths of fluorescence emission, fluorescence lifetimes, triplet lifetimes (in brackets the maximum absorption wavelength of the triplet states), and rate constants of triplet deactivation in air-equilibrated monoliths. [b]**PN** is not fluorescent. [c]Calculated from the PS amount and its absorbance in the monolith. A volume of approximately 0.44 cm^3 (mL) was considered to calculate the PS molar concentration. A relative uncertainty of 10% should be taken into account. [d]Estimated from DRUV spectra.

for **SG0-MB$^+$**. On the basis of the decay curves (inset of Figure 5a and b), several species were formed. For **SG0-NMB$^+$**, the triplet excited state was assigned to the transient spectrum observed at 65 and 250 ns and showing a maximum at 380 nm with two shoulders at 420 and 480 nm. Relative to solutions, the solid matrix induced a blue-shift of the triplet−triplet absorption spectrum by approximately 40 nm.[69] The transient spectrum measured 1 μs after the pulse is little different. Possibly, the absorption band arises from the superimposition of the triplet band and those of the semireduced (**NMB$^\bullet$**) and/or the semioxidized (**NMB$^{\bullet 2+}$**) forms of the dye. In **SG0-MV** materials, the results were quite similar. The triplet state was mainly responsible for the absorption band with a maximum at 380 nm observed 65 ns after the pulse. This spectrum resembles the one measured in MeOH solutions but it is however blue-shifted by approximately 40 nm. A second species observable in spectra measured 250 ns and 1 μs after the pulse builds up. This species is not firmly assigned but could more likely be attributed to radicals as for the other PSs. Confirming recent data on these PTZ dyes in solution, **MB$^+$** and **NMB$^+$** could react via electron transfer yielding PTZ$^{\bullet+}$ (and other ROS such as the superoxide anion, $O_2^{\bullet-}$), whereas in a protic environment such as silica, **MV** photoreactivity is limited to energy transfer to ground state oxygen for $^1O_2$ production.[69]

The triplet lifetime (Table 4) of supported **PN** (3.4 μs) was much longer than in aerated solutions, between 230 and 470 ns depending on the solvent,[49] but shorter than in deaerated solutions (approximately 40 μs).[71,79] For **SG0-MB$^+$** the triplet lifetime was 4.5 μs, compared to 12.5 and 0.28 μs measured in Ar-saturated and air-equilibrated ACN, respectively. Our results were close to those of Wetzler et al.,[19] who reported triplet lifetimes of 19 and <1 μs for dry and wet Nafion-supported **MB$^+$**, respectively. **NMB$^+$** triplet lifetime in monoliths (3.8 μs) was very close to the values recorded in oxygen-free ACN (3.7 μs), MeOH (4.8 μs), and water (2.5 μs).[69,80] For **MV**, the triplet lifetime value of 4.8 μs was closer to those measured in deaerated ACN (8.3 μs) and MeOH (5.9 μs) than in air-equilibrated solutions (approximately 200 ns). These values suggested a significant triplet lifetime increase when PSs are supported and thus a less efficient PSs triplet state quenching inside the matrix than in air-equilibrated solutions. Possibly the matrix stabilizes the transient state by decreasing the collisions between the excited molecules and the environment (liquid solvent vs silica). Also, a lower accessibility of molecular oxygen in the porous structure of silica relative to liquid solutions could result in a lower quenching of the transient state of the PS. Contrary to what observed for all the above-mentioned PSs, the triplet lifetime of supported **DBTP** (approximately 300 ns) was roughly the same as in air-equilibrated ACN.

To summarize, high quality transient absorption spectra of the studied PSs in silica were obtained. The transient spectra of supported **DBTP**, **DCA**, and **PN** were in good agreement with those recorded in solutions, whereas the T−T absorption spectra of the phenothiazine PSs were significantly blue-shifted

dx.doi.org/10.1021/am404175y | ACS Appl. Mater. Interfaces 2014, 6, 275−288

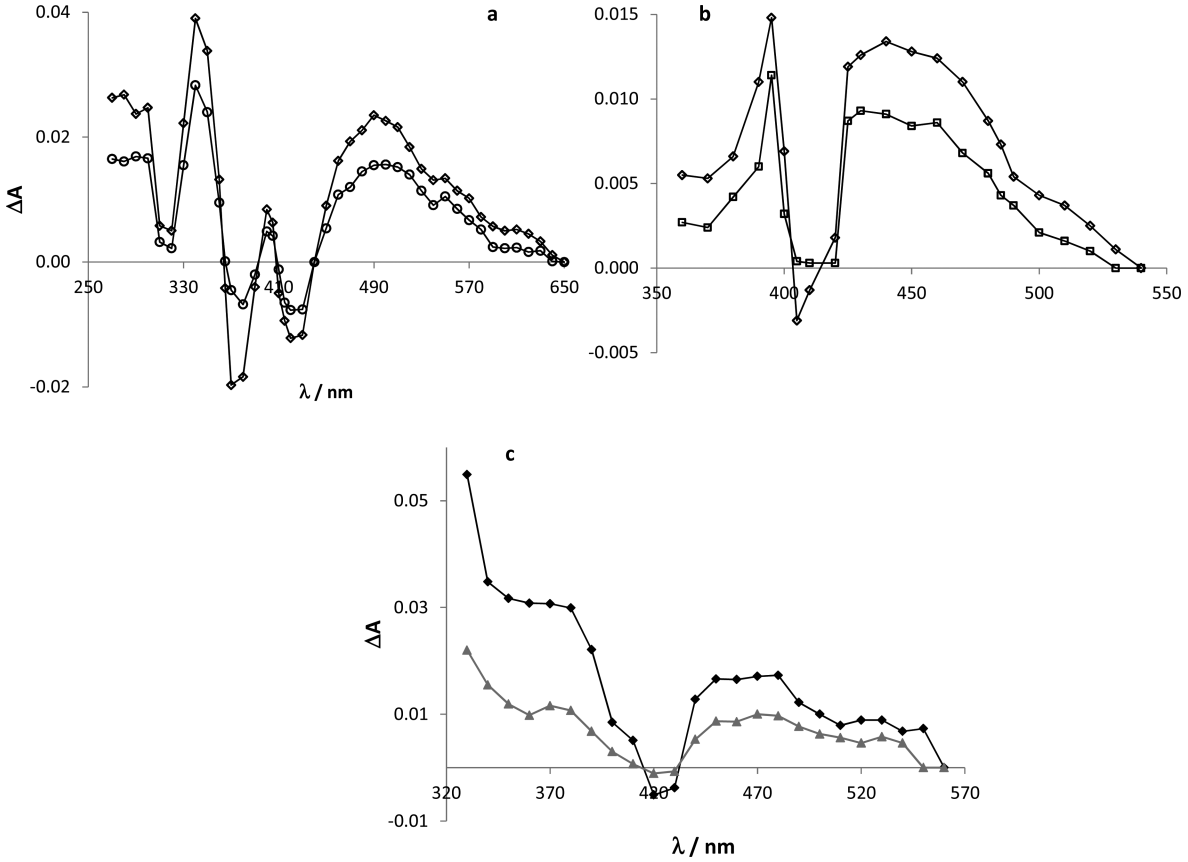

Figure 4. Time-evolution of the transient spectrum obtained by laser flash photolysis of (a) **SG0-PN** (80 ns, diamonds, and 1 μs, circles, after the laser pulse), (b) **SG0-DCA** (60 ns, diamonds, and 100 ns, squares, after the laser pulse), and (c) **SG0-DBTP** (50 ns, black diamonds, and 100 ns, gray triangles, after the laser pulse).

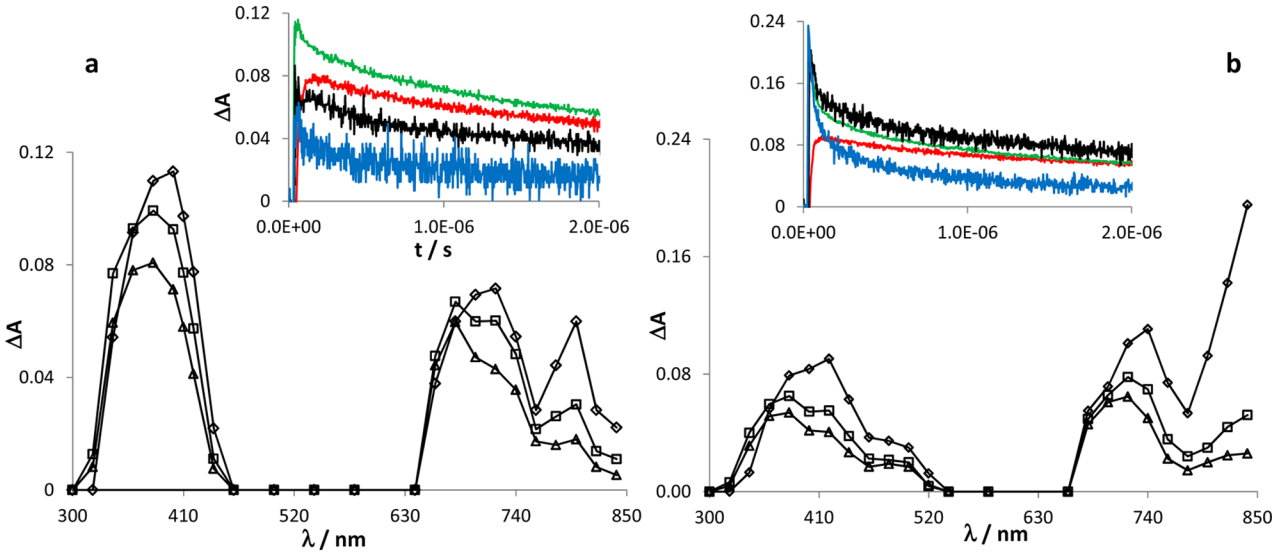

Figure 5. Time-evolution (65 ns, diamonds, 250 ns, squares, and 1 μs, triangles, after the laser pulse end) of the transient spectrum obtained by laser flash photolysis of **SG0-MV** (a) and **SG0-NMB**$^+$ (b). (insets) transient decays at different wavelengths: 340 (red), 420 (green), 740 (black), and 840 nm (blue).

(approximately 50 nm) relative to solutions. The triplet excited states were generally identified as the main transient species formed upon irradiation, even though for **MB**$^+$, **NMB**$^+$, and **MV** secondary mechanisms involving electron transfer reactions could be detected. Except for **DBTP**, the triplet lifetimes in silica appeared significantly longer than in air-equilibrated solutions.

Singlet Oxygen Detection. *Singlet Oxygen Lifetimes.* Singlet oxygen lifetimes (τ_Δ) in the monoliths were determined by time-resolved phosphorescence detection (TRPD).[54,55] Singlet oxygen phosphorescence decay traces observed for the series of **PN**-, **DBTP**-, and **RB-SG0** monoliths could be fitted with a single exponential function (equation SI 4, SI).

dx.doi.org/10.1021/am404175y | *ACS Appl. Mater. Interfaces* 2014, 6, 275−288

Table 5. Values of $^1O_2$ Lifetimes τ_Δ Derived from Monoexponential Decays in the Case of PN-, DBTP-, and RB-SG0 Monoliths[a]

PS (λ_{ex}/nm)	$\tau_{\Delta,1}/\mu s$	A_1/%	$\tau_{\Delta,2}/\mu s$	A_2/%	a_1/au[b]	$\Phi_{\Delta,rel}$ (Φ_Δ *in ACN*)[40,68]
SG0-PN (367)	20 ± 1	100				
	(24.7 ± 0.5)[25]	100			4.7 ± 0.3	1 (*1.00*)
	(24.0 ± 1)[c]	100				
SG0-DCA (367)	21.5 ± 0.8	100			3.3 ± 0.4	(1.02 ± 0.1)[26] (*0.30*)
	(22.5 ± 0.7)[25]	100				
	18 ± 1	100				0.9 ± 0.1
SG0-DBTP (367)	(24.4 ± 0.5)[26]	100			4.4 ± 0.3	(0.89 ± 0.04)[26]
	(18.4 ± 0.7)[c]	100				(*0.95*)
SG2-ACN-DBTP (367)	19 ± 1	100			2.7 ± 0.1	0.6 ± 0.1 (*0.95*)
SG0-RB (547)	15 ± 1	100			3.5 ± 0.2	0.6 ± 0.1 (*0.42*)
SG0-MV (547)[a]	14 ± 1	96	107 ± 30	4	2.1 ± 0.1	1.0 ± 0.1 (*0.60*)
SG0-NMB$^+$ (547)[a]	16 ± 1	95	136 ± 28	5	2.2 ± 0.1	0.6 ± 0.1 (*0.66*)

[a] $\tau_{\Delta,1}$ and $\tau_{\Delta,2}$ derived from biexponential decays in the case of **MV**- and **NMB$^+$-SG0** monoliths. [b] Slopes (a_1) of the variation of the intensity of the $^1O_2$ emission signal (S_{ss}) as a function of the fraction of photons absorbed by the PS (α_{PS}) (eq 1), quantum yields of $^1O_2$ production relative to PN ($\Phi_{\Delta,rel}$). The absorbances of all the tested monoliths are listed in Table SI 1, SI. [c] Data measured under our current conditions on the 6-year old samples from refs 25 or from 26.

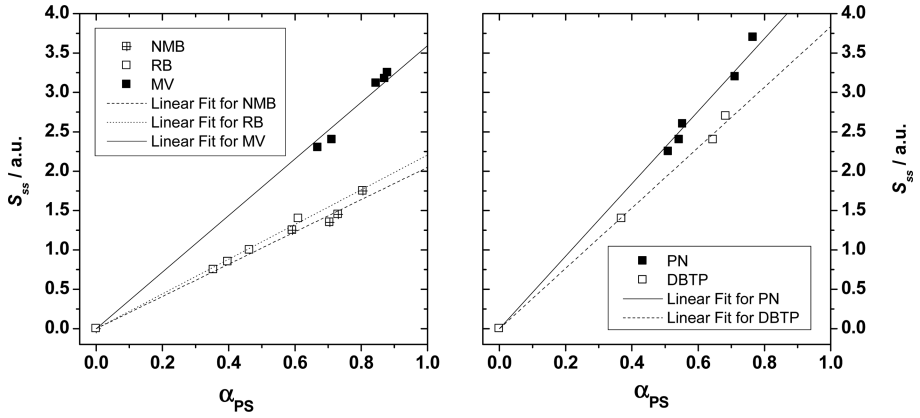

Figure 6. Variation of the intensity of the $^1O_2$ emission signal (S_{ss}) for SG0-monoliths containing **NMB$^+$**, **RB** and **MV** (left), and **PN** and **DBTP** (right), as a function of the fraction of photons absorbed by the PS (α_{PS}) in the monoliths.

The measured τ_Δ in the newly prepared **SG0-DBTP**, **-PN**, and **-DCA** and **SG2-ACN-DBTP** monoliths were in the range 18−21.5 μs, slightly lower than those previously reported (Table 5).[25] The measured τ_Δ for **SG0-RB** was slightly lower (15 μs) but, in contrast to the other samples, **RB** was not homogeneously distributed in the monolith. Decay traces observed for **SG0-MV** and **SG0-NMB$^+$** could only be fitted with a biexponential function (Equation SI 5, SI). The contribution of the decay with the longest lifetime (above 100 μs) was however weak (≤5%). Control experiments carried out in ACN solution confirmed that such a behavior was specific for the silica matrix. Two hypotheses may be proposed for explaining the apparent $^1O_2$ biexponential decay observed for these samples: (i) the PSs may locate in two different sites with different properties for $^1O_2$ deactivation, and rate of $^1O_2$ exchange between these two sites is much slower than $^1O_2$ decay in each site; (ii) electron transfer from the PS triplet excited state to molecular oxygen, favored by the matrix, could occur in parallel with energy transfer and recombination of the radical ions pair ($PS^{\bullet+}$ and $O_2^{\bullet-}$) might produce both $^3O_2$ and $^1O_2$; in this case the apparently longer lived $^1O_2$ emission would be in fact delayed $^1O_2$ production. The second hypothesis could however be excluded: we recently outlined for **NMB$^+$** and **MV** in solution that the electron transfer reaction yielding $PS^{\bullet+}$ and $O_2^{\bullet-}$ is negligible compared to singlet oxygen generation (for **MV**, electron transfer may only occur in nonprotic media).[69] It may be noticed that τ_Δ of the most significant short-lived component is smaller in the case of the phenothiazine dyes (14−16 μs) than in the case of **PN** and **DBTP** (18−20 μs). This behavior could be assigned to (i) a more significant singlet oxygen total quenching (k_t^{PS}) by **NMB$^+$** and **MV** than by the other PSs or (ii) to different optical properties of the silica matrices.

Singlet Oxygen Production and Quantum Yields. The quantum yields of $^1O_2$ production (Φ_Δ) by the PSs inside the monoliths were determined by SSPD,[50−52] measuring the $^1O_2$ luminescence signals (S_{ss}) at various PS concentrations using **PN** as a reference sensitizer (Φ_Δ close to 1 in a large variety of solvents).[43,49,79,82,83] The relation between the signal intensity S_{ss} and Φ_Δ is given by:

$$S_{ss} = KP_{a,PS}\Phi_\Delta\tau_\Delta = KP_0\alpha_{PS}\Phi_\Delta\tau_\Delta \quad (1)$$

where K is a proportionality factor (including geometric and electronic factors of the detection system, characteristics of the medium, and the $^1O_2$ radiative rate constant k_e).[55,83] $P_{a,PS}$ is the photon flux absorbed by the PS, given by eq 2:[84,85]

$$P_{a,PS} = P_0\alpha_{PS} = P_0\frac{(1 - 10^{-A_{tot}})A_{PS}}{A_{tot}} \quad (2)$$

where P_0 is the incident photon flux (section SI02 and equation SI 1, SI), α_{PS} is the fraction of incident photons absorbed by the PS, A_{tot} is the total absorbance at the wavelength of excitation

which includes the absorbance of the support (about 0.15 at 367 nm and nil at 547 nm) and that of the sensitizer (A_{PS}) and τ_Δ the $^1O_2$ lifetime (section SI04, SI).

The linearity of S_{SS} vs α_{PS} plots (Figure 6) attested that, in the range of concentrations used in this work (maximum absorbance of about 1 on the 5 mm optical path length of the monolith), the Beer−Lambert law was valid for all the PSs (diluted samples, absence of aggregation phenomena).[84,85] Moreover, these linear relationships showed that quenching of $^1O_2$ by the PS itself could be neglected ($k_t^{PS}[PS] \ll k_d$, eq SI 3, SI). The slopes a_1 of these plots ($= KP_0\Phi_\Delta\tau_\Delta$) were calculated. The ratio of the a_1 values obtained for each PS and the reference sensitizer (**PN**) allowed the determination of relative quantum yields of $^1O_2$ production ($\Phi_{\Delta,rel}$) using eq 3. Values of a_1 and ($\Phi_{\Delta,rel}$) for the different sensitizers are listed in Table SI 1, SI. For the calculation of $\Phi_{\Delta,rel}$, the $^1O_2$ lifetime was considered to be the same in all the monoliths (average of the values reported in Table 5).

$$\Phi_{\Delta,rel} = \frac{\Phi_\Delta^{PS}}{\Phi_\Delta^{R}} = \frac{a_1^{PS}}{a_1^{R}}\frac{\tau_\Delta^{R}}{\tau_\Delta^{S}}\frac{P_0^{R}}{P_0^{PS}} \quad (3)$$

To determine the effect of gas exchange on the singlet oxygen production in the monoliths, $^1O_2$ production irradiating **SG0-PN** materials ($A_{367\ nm} = 0.5$) was monitored under different gas environments. When Ar was let flow in situ for approximately 30 min above a monolith positioned on the optical bench for $^1O_2$ measurements, no significant change in the intensity of $^1O_2$ emission signals was noticed (Figure 7A,a). On the contrary,

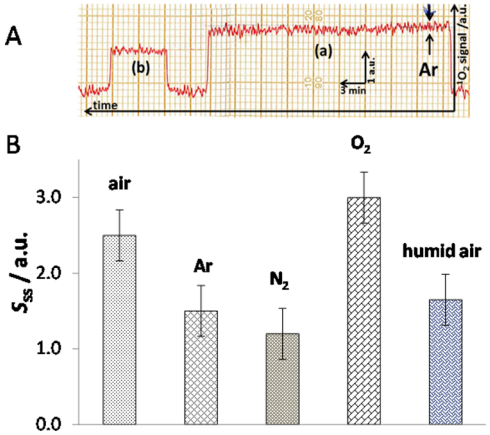

Figure 7. (A) Intensity of the $^1O_2$ signal as a function of time recorded for **SG0-PN** after: (a) Ar introduced in situ above the monolith for 30 min (the arrow shows the start of Ar injection); (b) injection of Ar in a flow cell during 30 min before the measurement. (B) Singlet oxygen emission signals as a function of the added gas in the flow cell during 30 min prior to the measurement of the $^1O_2$ signal (successive experiments on a **SG0-PN** material).

when the same monolith was placed in a cell in which a flow of Ar ($\approx$3 L min^{-1}) was circulated during 30 min (degassing ex-situ), $^1O_2$ production significantly dropped (approximately 40%, Figure 7A,b). This observation suggested that $^1O_2$ was mainly produced inside the monolith and not at the external solid−gas interface. This result could be expected since the total area of a monolith ($\approx$0.5 g) is approximately 27 × 10^7 vs 450 mm^2 of the external surface. In a second step, an **SG0-PN** sample was submitted during 30 min successively to a flow of about 3 L min^{-1} of N_2, O_2, and humid air. From these experiments, square signals were obtained showing that the production of $^1O_2$ was stable once the monolith was outside the flow cell and that gas exchange was negligible during the measurement time (5 min, Figure 7B). As observed for argon, N_2 led to a decrease in the $^1O_2$ emission signal by a factor of 2.3, larger than in the case of Ar (1.7), whereas O_2 led to a signal increase by a factor of 1.2 (Figure 7B). N_2 seemed to be more efficient than Ar in removing O_2 from the microporous structures. The positive effect of an increased concentration of oxygen on $^1O_2$ production (Figure 7B) may be explained by the increase of the probability of energy transfer from the triplet excited state of the PS to ground state oxygen ($^3O_2$). Humidification resulted in a decrease of the observed $^1O_2$ signal by a factor of 1.4 compared to the air-equilibrated monolith (Figure 7B), consistently with the well-known fact that O−H bonds efficiently quench $^1O_2$, resulting in a shorter τ_Δ in H_2O (approximately 4 μs) than in other solvents.[10,86] Moreover, the rate constant of $^1O_2$ emission (k_e) has also the smallest value in H_2O[55,83] and NIR radiation is efficiently absorbed by H_2O.

We also investigated the effect of the PS concentration in the monoliths on $^1O_2$ production at high absorbances. A very weak $^1O_2$ signal ($\approx$0.2 au, Figure SI 10, SI) was recorded with a **SG0-PN** monolith where the absorbance at the irradiation wavelength was $\gg$2. As a result of the high **PN** concentration, the penetration depth of the incident radiation inside this monolith was limited to a very thin layer. In this layer, the density of **PN** triplet excited states was high enough so that self-quenching (triplet−triplet annihilation) competed efficiently with quenching of the **PN** triplet excited state by O_2 to produce $^1O_2$.[87] In agreement with this hypothesis, after submitting this same monolith to a flow of about 3 L min^{-1} of O_2 during 60 min, the $^1O_2$ oxygen signal rose significantly ($\approx$1.3 au) and then decreased and stabilized ($\approx$0.7 au) after about 10 min (Figure SI 10, SI).

To analyze the effect of the monolith hydrophobicity on the efficiency of $^1O_2$ production, three **DBTP**-monoliths of approximately the same absorbance ($A \approx 0.3$ at 367 nm) but containing different percentages of OC groups (0%, **SG0**, 2% and 5%, **SG0-OC**) have been compared. Figure 8 shows that the $^1O_2$

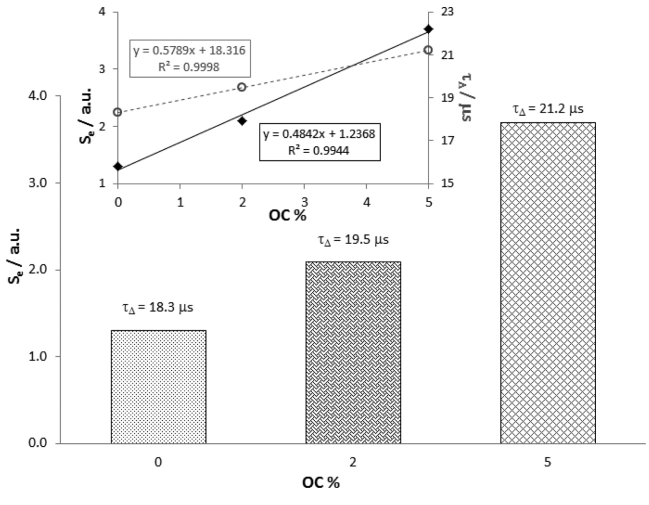

Figure 8. Intensity of the $^1O_2$ emission signal as a function of TMOS-OC % in **DBTP** monoliths of the same absorbance ($A \approx 0.3$ at 367 nm) in ambient air. Linear plots of $^1O_2$ signals intensity (S_{ss}, black line, diamonds) and $^1O_2$ lifetime (τ_Δ, secondary axis, gray dotted line, circles) as functions of OC %.

emission signals and $^1O_2$ lifetimes linearly increased with increasing TMOS-OC percentages. An increase of the S_{ss}/τ_Δ

dx.doi.org/10.1021/am404175y | ACS Appl. Mater. Interfaces 2014, 6, 275−288

ratio with OC% was also noticed, meaning that the increase of the signal intensity with increasing hydrophobicity was more significant than the parallel increase of τ_Δ. Besides, a signal intensity enhancement might also be due to (i) an increase of the value of k_e (rate constant of $^1O_2$ emission) as could be expected if the monolith becomes more hydrophobic;[55,83] (ii) a decrease of the refractive index of the monolith; (iii) a decrease in the NIR absorption of the monolith in the wavelength range of $^1O_2$ emission (1240−1300 nm); this was however not the case, since the transmittance spectra of the monoliths (Figure SI 11, SI) showed that NIR absorption slightly increased from 0% to 5% of TMOS-OC). In summary, the significant increase of $^1O_2$ signal intensity with TMOS-OC% (Figure 8) most probably reflected an increase of both k_e and Φ_Δ.

To summarize, for all the studied PSs, high relative singlet oxygen quantum yields $\Phi_{\Delta,rel}$ (0.6−1.0) were determined directly at the gas−solid interface. Table 5 also highlights a strong increase of Φ_Δ from ACN to silica monoliths for **DCA**, **MV**, and **RB**. Noticeably, despite its very short triplet lifetime (0.3 μs), **SG0-DBTP** shows a high Φ_Δ probably reflecting a highly efficient energy transfer to oxygen, already evidenced in solution and not significantly modified in the silica matrix.[40] Singlet oxygen lifetimes in the monoliths were in the range 15−21 μs, higher than in water (7 μs) and methanol (10 μs), and may be compared to literature data for air-equilibrated polyurethane (17 μs),[88] Nafion-Na (85 μs),[19] porphyrin-LDH-composites (32−55 μs),[22] and oxygen-equilibrated extensively dried silica (64 μs)[19] or zeolite (7.9 μs).[89] Steady-state singlet oxygen experiments with N_2, O_2, or air also demonstrate that the gaseous exchange inside the materials lies in the tenth of minutes time-range: the decrease of $^1O_2$ emission when changing oxygen for nitrogen was only observed after 30 min under N_2 flow. This result stems from the high surface area and porosity of the silica monoliths (555−730 $m^2\ g^{-1}$).

Photooxidation Activity. The efficiency of the PSs containing monoliths for the solvent-free photooxidation (PO) of DMS was investigated. The mechanism of the photosensitized oxidation of sulfides is well-known and described in detail in the the literature.[24,38,90−92] In case of singlet oxygen addition, sulfoxides and sulfones are the main products (DMSO and $DMSO_2$ if DMS is used as reactant). Side-products (dimethyldisulfide, DMDS, and *S*-methyl methanethiosulfonate, MMTS) can arise from C−S bond cleavage after the formation of the sulfide radical cation.

For this study a first adsorption step in the dark was carried out to saturate the silica monoliths with DMS. The saturation time varied between 22 h for the monoliths with the lowest specific surface area and 56 h for the more porous monoliths. The DMS saturation profiles with dried and H_2O-presaturated monoliths (Figure 9) could be compared and suggested that the airflow gently dragged off the adsorbed water during this saturation step. These results imply that the highly porous monoliths are excellent adsorbents for DMS. In Figure 9, a typical profile of DMS concentration variation vs irradiation time is reported. The conversion and initial rates for each irradiation cycle are summarized in Table 6. A striking drop of DMS concentration to approximately 20 ppmV occurred as soon as the lamps were switched on, before beginning to slowly increase. No other product except DMS was detected in the gas phase all along the experiments. As soon as the lamps were switched off after 24 h, the DMS concentration increased in two steps: very quickly to 150 ppmV and slowly in a second step to 200 ppmV, suggesting two adsorption sites. For **SG0-DBTP**, the initial consumption

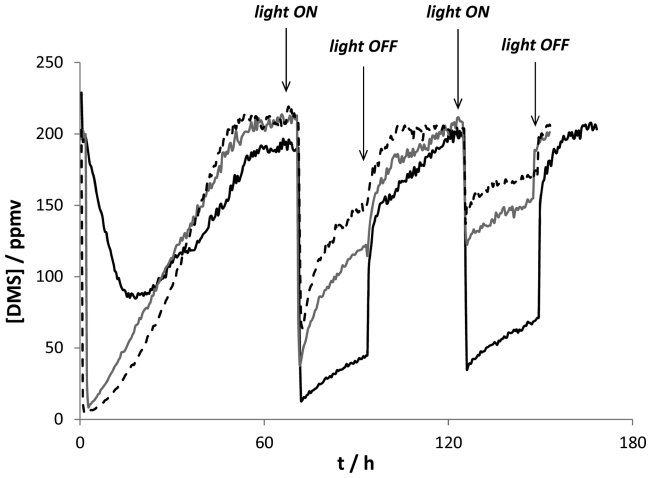

Figure 9. DMS concentration variation during photooxidation tests for a water-saturated **SG0-ACN-DBTP** monolith (black solid line), a dried **SG0-RB** monolith (dashed black line), and a dried **SG0-NMB$^+$** monolith (gray line). Reaction conditions: 100 mL min^{-1} (air flow), 200 ppmv (DMS concentration), room temperature. Irradiation wavelength: 420 nm for **SG0-ACN-DBTP** and 575 for **SG0-RB** and **SG0-NMB$^+$**.

rate (v_0) was noticeably much higher for the second cycle than for the first one, contrary to all the other materials most prone to photobleaching (Table 6). It is worth noticing that the DMS concentration at the beginning of the second irradiation cycle was always the same as the DMS concentration reached at the end of the first cycle, as if the strong adsorption of the oxidation products on silica limited the amount of DMS that could be adsorbed, and hence the total conversion during the second cycle.

DMSO was identified as the main product along with $DMSO_2$ formed in smaller amounts and DMDS and MMTS detected as traces (Figures SI 13−15, SI). No obvious differences in the photoproducts distribution were noticed between the different materials: it can be concluded that with all the PSs the reaction mainly proceeded through singlet oxygen formation by energy transfer and its subsequent addition to DMS. Electron transfer mechanisms (type I reactions) are thus secondary for the photooxidation of DMS under our experimental conditions with all included PSs, in agreement with the photophysical data obtained for these PSs in solution. We recently pointed out that **DBTP** in solution has an extremely efficient quantum yield of intersystem crossing and that photoinduced electron transfer is not possible with most of substrates once the triplet excited state is populated. With **DCA**, on the contrary, photoinduced electron transfer to either the singlet and the triplet excited state can more easily occur.[40] In the PTZ series, we pointed out for **MB$^+$** and **NMB$^+$** that the formation of the radical cation of the PSs could be obtained under excitation whatever the solvent. This photophysical mechanism was however observed to a much lower extent relative to triplet formation inducing type II reactions and $^1O_2$ generation. For **MV**, photoinduced electron transfer from the triplet excited state of the PS to molecular oxygen, with subsequent generation of superoxide radical anion, was only observed in aprotic media and was strongly disfavored in the presence of free H^+.[69] Additional photochemical studies involving other substrates (out of the scope of this work) would be needed to get any evidence of type I pathways and of the involvement of other ROS in addition to singlet oxygen, both in solution and in the supported materials. However, this latter

Table 6. Photooxidation Activity of Some SG0 Materials for the Sensitized Oxidation of DMS[a]

PS	PS amount/ mol g^{-1}	P/ mW cm^{-2}	conversion cycle 1/%	conversion cycle 2/%	initial rate cycle 1/ppm V h^{-1}	initial rate cycle 2/ppm V h^{-1}	bleaching/%
DBTP[b]	1.6×10^{-7}	16.7	51 (3.1)	40 (2.4)	−27	−120	27
DCA[b]	9.4×10^{-8}	27.6	26 (0.9)	11 (0.4)	−78	−25	40
PN[b]	5.7×10^{-8}	33.6	35 (1.0)	22 (0.7)	−40	−32	62
RB[c]	2.6×10^{-7}	13.1	42 (3.2)	19 (1.5)	−218	−140	95
MB^+[c]	4.7×10^{-7}	16.5	27 (1.6)	17 (1.0)	−225	−28	65
NMB^+[c]	8.5×10^{-8}	15.1	56 (3.7)	33 (2.2)	−430	−225	90
MV[c]	5.0×10^{-7}	16.2	41 (2.5)	9 (0.6)	−195	−102	90

[a]The absorbed photon flux was estimated using the following equation: $P_{a,\lambda} = \sum_\lambda P_{0,\lambda}(1 - 10^{-A_\lambda})$ considering absorption spectra of **SG0** materials before the photoactivity tests and the photon flux emitted by the lamps (λ > 350 nm). In the conversion columns, the values normalized to the absorbed photon flux are reported in brackets. Bleaching percentage was estimated from DRUV-Vis spectra recorded before and after the two irradiation cycles. [b]Irradiation at 420 nm. [c]Irradiation at 575 nm.

Table 7. Photooxidation Activity of Some DBTP-Derived Silica Monoliths for the Sensitized Oxidation of DMS[a]

monolith	PS amount/mol g^{-1}	S_a/m^2 g^{-1} (% mesopores)	P/mW cm^{-2}	conversion/%	initial rate cycle 1/ppm V h^{-1}	bleaching/%
SG0-OC 5%	9.2×10^{-8}	555 (23)	41.5	38 (0.9)	−385	18
SG0-ACN	2.0×10^{-7}	730 (30)	43.4	88 (2.0)	−455	3
SG0-ACN[b]	2.0×10^{-7}	730 (30)	43.4	86 (2.0)	−405	3
SG2-ACN	5.0×10^{-7}	660 (38)	40.7	83 (2.0)	−305	25

[a]PS concentration, specific surface area (percentage of mesopores in brackets), absorbed photon flux (see Table 6), percentage conversion, and, in brackets, percentage conversion normalized by the absorbed photon flux, bleaching percentage (estimated from DRUV-vis spectra, SI). [b]Water-saturated sample: approximately 100 mg of water were adsorbed before the photooxidation test.

reaction mechanism would probably not be the favored one according to the described available data.

All the supported PSs efficiently oxidized DMS under visible-light irradiation (conversions 26−56% for the first irradiation cycle and 9−40% for the second cycle, Table 6). Considering the DMS conversion normalized to the photon flux absorbed by the PS, for both irradiation cycles the most efficient materials were **SG0-DBTP**, **SG0-NMB^+**, and **SG0-RB** (Table 6), while the less efficient were **SG0-DCA** and **SG0-PN**. This is contrary to what one could expect from the data relative to singlet oxygen production. **DBTP** was the most bleaching resistant PS (<30%), followed by **DCA** (40%) and **PN** (62%). The other PSs were not expected to be very resistant under such radiant power and the bleaching percentages were very high (90% and 95%, respectively, for **NMB^+/MV** and **RB**). Considering both conversion and bleaching, it emerged that the best material for the photooxidation of DMS was **SG0-DBTP**. From the DMS concentration profile, we can assume that for this photooxidation reaction to take place, the close proximity of the excited sensitizer, the pollutant and oxygen was needed. Consequently, since the PS was firmly anchored to the silica structure, the probability of reaction between the organic sensitizer and the ROS could be higher than in solution, where both PS and $^1O_2$ could freely move in the system. Hence, the photobleaching of the PS could be slightly enhanced in silica matrices relative to solutions, although an accurate comparison of photobleaching rates was not carried out. Nonetheless, from the DMS concentration variation during the photooxidation tests and the long duration of irradiation, it emerged that the self-oxidation of the embedded PSs was negligible compared to the efficient conversion of DMS.

Given the high efficiency and photostability of **SG0-DBTP**, we then focused on the influence of silica modifications and of **DBTP** grafting on the efficiency of DMS oxidation (Table 7). **SG0-ACN** materials were the most efficient and stable under irradiation. The effect of grafting (**SG2-ACN-DBTP**) on the photoactivity was negligible but surprisingly resulted in a lower stability under irradiation. Monolith saturation with water did not affect the photoactivity of the material. It was easily outlined that the highest normalized conversions corresponded to the highest specific surface areas (normalized conversions of 0.9 and 2.0 for 555 and 730 m^2 g^{-1} S_a, respectively) while the influence of the micro/mesoporosity seemed less important. Silica functionalization with octyl groups decreased both the conversion (related to S_a decrease) and the photostability of the PS: for these oxidation conditions, it is thus not worthwhile increasing the hydrophobicity of the silica matrix. On the contrary, ACN as a cosolvent had a positive effect on the activity and PS stability under irradiation, probably related to an increase of the specific surface area.

The efficiency of DMS photooxidation was thus more related to the specific surface area of the matrix than to the Φ_Δ of the sensitizer. Despite the slow sensitivity (in the tenth of minutes range) of the singlet oxygen signal to a change from air to N_2 or O_2, quenching of the triplet states of the PSs by ground state oxygen (located in the pores of the silica matrix, together with the PS) was highly efficient, as shown by the relatively high values of Φ_Δ. Taking into account the diffusion coefficient (0.18 cm^2 s^{-1}) and the lifetime (τ_Δ 54 ms)[93] of $^1O_2$ in air, the diffusion length (d) of $^1O_2$ is calculated to be 2.4 mm from eq 4:

$$d = \sqrt{6D\tau_\Delta} \quad (4)$$

The same calculation in silica gives a diffusion distance of 5×10^{-3} nm (with diffusion coefficient $D = 2.2 \times 10^{-15}$ cm^2 s^{-1} for SiO_2 coatings prepared by the sol−gel method[94] and τ_Δ of 20 μs). This result means that both ground state and singlet oxygen are able to diffuse in the pores and that the quenching of the PSs triplet state predominantly occurs at the gas−solid interface. Once formed, $^1O_2$ is free to diffuse across the silica pores, the diameter of which is much smaller than its diffusion distance. If DMS is previously adsorbed and confined inside silica, singlet oxygen can readily add on it as soon as it is produced, explaining the very fast decay of DMS adsorption as soon as the irradiation begins. The high surface area of silica plays thus an important role in the conversion of DMS: the highly efficient adsorption of the

sulfide inside the matrix allows the proximity between the PS, DMS, and oxygen, inducing efficient $^1O_2$ formation and its fast addition to the adsorbed sulfide. This scheme also accounts for the decrease of reaction rate due to adsorbed oxidation products (sulfoxide and sulfone), which reduce DMS adsorption and oxygen diffusion. The complementary role of the matrix for achieving the efficient conversion of volatile pollutants should thus be considered in the analysis of the photooxidation properties of sensitizers supported on solid matrices.

CONCLUSION

Embedded or grafted PSs in silica monoliths are able to photogenerate $^1O_2$ molecules that react very efficiently on sulfides in a solvent-free process. These silica monoliths are also suitable for the easy acquisition of steady-state or time-resolved absorption/emission spectra directly in the solid samples, without use of any suspensions. The biexponential fluorescence decay of most of the silica-embedded PSs suggested two locations of the PSs with different properties and oxygen content.

High quality transient absorption spectra were obtained. A strong effect of the silica matrix was evidenced on the transient spectrum of all the phenothiazine PSs: the triplet excited state absorption bands are shifted by at least 40 nm relative to the spectra recorded in solution. For the other PSs the triplet absorption spectra are not shifted relative to solution. The triplet lifetimes in silica appear much longer than in air-equilibrated solvents and in some cases close to the lifetimes measured in deaerated solutions. Only for **DBTP**, the triplet lifetime is similar to aerated ACN solutions.

Triplet states are efficiently quenched by oxygen as shown by the high singlet oxygen quantum yields (Φ_Δ 0.6−1.0) determined directly at the gas−solid interface. It may thus be concluded that PS molecules included in the matrix are accessible to gaseous oxygen present in the silica network.

No evident correlations between the production of singlet oxygen in silica monoliths and the corresponding photoactivity for DMS oxidation could be pointed out: the addition of hydrophobic octyl groups for example increased Φ_Δ while decreasing the photooxidation efficiency, together with a decreased specific surface area. It seemed that in the experimental time scale of this work, the structural and porous properties of silica affected the photooxidation activity more than the efficiency of $^1O_2$ production by the PS itself. From the analysis of the diffusion distance of oxygen inside the material, it was concluded that singlet oxygen was very efficiently produced at the gas−solid interface and was free to diffuse inside the silica pores. For an efficient energy transfer to oxygen, the PS concentration inside silica has to be low enough to avoid triplet−triplet annihilation. In the presence of adsorbed water inside silica, singlet oxygen is efficiently quenched. Nonetheless, in our experimental conditions for DMS photooxidation, water was dragged off the solid by the air flux and could not affect the photochemical activity.

Transparent silica monoliths can act both as suitable supports for the characterization of the reactive species involved in the photochemical processes and as efficient microreactors for photosensitized oxidation reactions in a medium behaving like a "solid solution". The stability of the materials over time (6 y) was demonstrated. Among the various PSs tested, the three phenothiazine dyes, **MB**$^+$, **NMB**$^+$, and **MV** were very efficient but prone to photobleaching, while **DBTP** was more active and more resistant to photobleaching. Grafted **DBTP** also presents a high efficiency but with a slightly reduced resistance to bleaching. Consistently to what was observed in solutions, **MV** results to be much more resistant to irradiation in more acidic silica than in conventional monoliths.

ASSOCIATED CONTENT

Supporting Information

Chemicals and syntheses; procedures for singlet oxygen ($^1O_2$) detection; procedure for photooxidation (PO) tests; setup for PO tests; emission spectra of the lamps used for PO tests; DRUV spectra of **DBTP** based materials; fluorescence spectra of **SG0-DCA**, **SG0-NMB**$^+$, **SG0-MV**; transient absorption spectra recorded for **SG0-MB**$^+$ and **SG0-RB**; transient decays recorded for **SG0-DBTP** and **SG0-ACN-DBTP**; analysis for the determination of $^1O_2$ lifetime; $^1O_2$ luminescence decays for **SG0-PN** and **SG0-MV**; PSs absorbance in various monoliths and corresponding relative quantum yields of $^1O_2$ production; effect of PS concentration and different gaseous atmospheres on $^1O_2$ luminescence signal; NIR transmittance spectra of **SG0-OC-DBTP** monoliths; monoliths aging effect on $^1O_2$ lifetime; air flow effect on DMS conversion during PO tests; photobleaching of **DBTP** based materials during the PO tests; gas chromatography of desorbed PO products (**SG0-NMB**$^+$ and **SG0-MV**); mass spectra of desorbed PO products (DMSO and $DMSO_2$). This material is available free of charge via the Internet at http://pubs.acs.org.

AUTHOR INFORMATION

Corresponding Author

*Tel.: +33 5 59407579. Fax: +33 5 5940622. E-mail: sylvie.lacombe@univ-pau.fr.

Author Contributions

$^\perp$E.A. and F.R. made an equivalent contribution to this work.

Notes

The authors declare no competing financial interest.

ACKNOWLEDGMENTS

The authors greatly acknowledge the Agence Nationale de la Recherche (ANR, programme Blanc 2010 (10-BLAN-0803) for funding, the Ministère de l'Enseignement Supérieur et de la Recherche (MESR) for a grant to F.R., and Virginia Martínez and Iñigo Lopez Arbeloa for fluorescence lifetime measurements.

REFERENCES

(1) DeRosa, M. C.; Crutchley, R. J. *Coord. Chem. Rev.* **2002**, *233*, 351−371.
(2) Lacombe, S.; Pigot, T. In *New materials for sensitized photooxygenation*; Albini, A. Ed.; The Royal Society of Chemistry: Cambridge, 2010; Vol. *38*, p 307.
(3) Miranda, M. A.; Garcia, H. *Chem. Rev.* **1994**, *94*, 1063−1089.
(4) Hoffmann, N. *ChemSusChem* **2012**, *5*, 352−371.
(5) Oelgemöller, M.; Jung, C.; Mattay, J. *Pure Appl. Chem.* **2007**, *79*, 1939−1947.
(6) Jesenská, S.; Plíštil, L.; Kubát, P.; Lang, K.; Brožová, L.; Popelka, Š.; Szatmáry, L.; Mosinger, J. *J. Biomed. Mater. Res. A* **2011**, *99A*, 676−683.
(7) Rolim, J. P. M. L.; de-Melo, M. A. S.; Guedes, S. F.; Albuquerque-Filho, F. B.; de Souza, J. R.; Nogueira, N. A. P.; Zanin, I. C. J.; Rodrigues, L. K. A. *J. Photochem. Photobiol. B: Biol.* **2012**, *106*, 40−46.
(8) Hocine, O.; Gary-Bobo, M.; Brevet, D.; Maynadier, M.; Fontanel, S.; Raehm, L.; Richeter, S.; Loock, B.; Couleaud, P.; Frochot, C. *Int. J. Pharm.* **2010**, *402*, 221−230.
(9) Jia, X.; Jia, L. *Curr. Drug Metab.* **2012**, *13*, 1119−1122.
(10) Wilkinson, F.; Helman, W. P.; Ross, A. B. *J. Phys. Chem. Ref. Data* **1995**, *24*, 663−677.
(11) Aebisher, D.; Zamadar, M.; Mahendran, A.; Ghosh, G.; McEntee, C.; Greer, A. *Photochem. Photobiol.* **2010**, *86*, 890−894.

(12) Benabbou, A. K.; Guillard, C.; Pigeot-Remy, S.; Cantau, C.; Pigot, T.; Lejeune, P.; Derriche, Z.; Lacombe, S. *J. Photochem. Photobiol. A: Chem.* **2011**, *219*, 101−108.
(13) Horsa, S.; Perez, K.; Miksovska, J. *J. Photochem. Photobiol. A: Chem.* **2011**, *221*, 84−89.
(14) Lee, J.; Mackeyev, Y.; Cho, M.; Wilson, L. J.; Kim, J. H.; Alvarez, P. J. *Environ. Sci. Technol.* **2010**, *44*, 9488−9495.
(15) Nicole, L.; Rozes, L.; Sanchez, C. *Adv. Mater.* **2010**, *22*, 3208−3214.
(16) Amore, S.; Lagorio, M. G.; Dicelio, L. L.; San Romàn, E. *Prog. React. Kinet. Mech.* **2001**, *26*, 159−177.
(17) Ma, D.; Kell, A. J.; Tan, S.; Jakubek, Z. J.; Simard, B. *J. Phys. Chem. C* **2009**, *113*, 15974−15981.
(18) Mosinger, J.; Lang, K.; Plistil, L.; Jesenska, S.; Hostomsky, J.; Zelinger, Z.; Kubat, P. *Langmuir* **2010**, *26*, 10050−10056.
(19) Wetzler, D. E.; García-Fresnadillo, D.; Orellana, G. *Phys. Chem. Chem. Phys.* **2006**, *8*, 2249−2256.
(20) Loponov, K.; Goller, B.; Moskalenko, A.; Kovalev, D.; Lapkin, A. *J. Photochem. Photobiol. A: Chem.* **2010**, *211*, 74−77.
(21) Rossi, L. M.; Silva, P. R.; Vono, L. L. R.; Fernandes, A. U.; Tada, D. B.; Baptista, M. S. *Langmuir* **2008**, *24*, 12534−12538.
(22) Lang, K.; Bezdicka, P.; Bourdelande, J. L.; Hernando, J.; Jirka, I.; Kafunkova, E.; Kovanda, F.; Kubat, P.; Mosinger, J.; Wagnerova, D. M. *Chem. Mater.* **2007**, *19*, 3822−3829.
(23) Cojocaru, B.; Laferriere, M.; Carbonell, E.; Parvulescu, V.; Garcia, H.; Scaiano, J. C. *Langmuir* **2008**, *24*, 4478−4481.
(24) Latour, V.; Pigot, T.; Mocho, P.; Blanc, S.; Lacombe, S. *Catal. Today* **2005**, *101*, 359−367.
(25) Cantau, C.; Pigot, T.; Manoj, N.; Oliveros, E.; Lacombe, S. *ChemPhysChem* **2007**, *8*, 2344−2353.
(26) Lacombe, S.; Soumillion, J.-P.; El Kadib, A.; Pigot, T.; Blanc, S.; Brown, R.; Oliveros, E.; Cantau, C.; Saint-Cricq, P. *Langmuir* **2009**, *25*, 11168−11179.
(27) Saint-Cricq, P.; Pigot, T.; Nicole, L.; Sanchez, C.; Lacombe, S. *Chem. Commun.* **2009**, 5281.
(28) Cantau, C.; Pigot, T.; Brown, R.; Mocho, P.; Maurette, M. T.; Benoit-Marquié, F.; Lacombe, S. *Appl. Catal. B: Environ.* **2006**, *65*, 77−85.
(29) Guli, M.; Li, X.; Zhang, K.; Chi, Y. *J. Sol−Gel Sci. Technol.* **2010**, *54*, 329−334.
(30) Adachi, I.; Tabata, M.; Kawai, H.; Sumiyoshi, T. *Nucl. Instrum. Methods Phys. Res. Sect. Accel. Spectrometers Detect. Assoc. Equip.* **2011**, *639*, 222−224.
(31) Kumar, P.; Guliants, V. V. *Microporous Mesoporous Mater.* **2010**, *132*, 1−14.
(32) Latthe, S. S.; Imai, H.; Ganesan, V.; Kappenstein, C.; Venkateswara Rao, A. *J. Sol−Gel Sci. Technol.* **2009**, *53*, 208−215.
(33) Gao, C.; Che, S. *Adv. Funct. Mater.* **2010**, *20*, 2750−2768.
(34) Gay, D. S. F.; Fernandes, T. H. M.; Amavisca, C. V.; Cardoso, N. F.; Benvenutti, E. V.; Costa, T. M. H.; Lima, E. C. *Desalination* **2010**, *258*, 128−135.
(35) Fukaya, N.; Haga, H.; Tsuchimoto, T.; Onozawa, S.; Sakakura, T.; Yasuda, H. *J. Organomet. Chem.* **2010**, *695*, 2540−2542.
(36) Bolshan, Y.; Tomaszewski, M. J.; Santhakumar, V. *Tetrahedron Lett.* **2007**, *48*, 4925−4927.
(37) Gu, X.; Li, X.; Chai, Y.; Yang, Q.; Li, P.; Yao, Y. *Green Chem.* **2013**, *15*, 357−361.
(38) Baciocchi, E.; Del Giacco, T.; Elisei, F.; Gerini, M. F.; Guerra, M.; Lapi, A.; Liberali, P. *J. Am. Chem. Soc.* **2003**, *125*, 16444−16454.
(39) Bonesi, S. M.; Fagnoni, M.; Albini, A. *Eur. J. Org. Chem.* **2008**, *2008*, 2612−2620.
(40) Ronzani, F.; Arzoumanian, E.; Blanc, S.; Bordat, P.; Pigot, T.; Cugnet, C.; Oliveros, E.; Sarakha, M.; Richard, C.; Lacombe, S. *Phys. Chem. Chem. Phys.* **2013**, *15*, 17219−17232.
(41) Lamberts, J. J. M.; Neckers, D. C. *J. Am. Chem. Soc.* **1983**, *105*, 7465−7467.
(42) Mills, A.; Hazafy, D.; Parkinson, J. A.; Tuttle, T.; Hutchings, M. G. *J. Phys. Chem. A* **2009**, *113*, 9575−9576.
(43) Schmidt, R.; Tanielian, C.; Dunsbach, R.; Wolff, C. *J. Photochem. Photobiol. A: Chem.* **1994**, *79*, 11−17.
(44) Wainwright, M.; Giddens, R. M. *Dyes Pigmen.* **2003**, *57*, 245−257.
(45) Otsuki, S.; Taguchi, T. *Bull. Chem. Soc. Jpn.* **1996**, *69*, 2525−2531.
(46) Wainwright, M. *Int. J. Antimicrob. Agents* **2000**, *16*, 381−394.
(47) Brinker, C. J.; Scherer, G. W. *Sol−Gel Science: The Physics and Chemistry of Sol-Gel Processing*; Gulf Professional Publishing, 1990.
(48) Braun, A. M.; Oliveros, E. *Pure Appl. Chem.* **1990**, *62*, 1467−1476.
(49) Martí, C.; Jürgens, O.; Cuenca, O.; Casals, M.; Nonell, S. *J. Photochem. Photobiol. Chem.* **1996**, *97*, 11−18.
(50) Aminian-Saghafi, T.; Nasini, G.; Caronna, T.; Braun, A. M.; Oliveros, E. *Helv. Chim. Acta* **1992**, *75*, 531−538.
(51) Thomas, A. H.; Lorente, C.; Capparelli, A. L.; Martinez, C. G.; Braun, A. M.; Oliveros, E. *Photochem. Photobiol. Sci.* **2003**, *2*, 245−250.
(52) Cabrerizo, F. M.; Laura Dántola, M.; Petroselli, G.; Capparelli, A. L.; Thomas, A. H.; Braun, A. M.; Lorente, C.; Oliveros, E. *Photochem. Photobiol.* **2007**, *83*, 526−534.
(53) Nonell, S.; Braslavsky, S. E. In *Methods in Enzymology*; Lester Packer, H. S., Ed.; Academic Press, 2000; Vol. *319*, pp 37−49.
(54) Boneva, M.; Ivanov, S. K.; Oliveros, E.; Braun, A. M. *J. Photochem. Photobiol. A: Chem.* **1992**, *68*, 343−351.
(55) Martinez, L. A.; Martínez, C. G.; Klopotek, B. B.; Lang, J.; Neuner, A.; Braun, A. M.; Oliveros, E. *J. Photochem. Photobiol. B: Biol.* **2000**, *58*, 94−107.
(56) Benoit-Marquié, F.; Wilkenhöner, U.; Simon, V.; Braun, A. M.; Oliveros, E.; Maurette, M.-T. *J. Photochem. Photobiol. A: Chem.* **2000**, *132*, 225−232.
(57) McKelvey, J. M.; Hoelscher, H. E. *Anal. Chem.* **1957**, *29*, 123−123.
(58) Shendage, D. M.; Fröhlich, R.; Haufe, G. *Org. Lett.* **2004**, *6*, 3675−3678.
(59) Hegde, N. D.; Venkateswara Rao, A. *Appl. Surf. Sci.* **2006**, *253*, 1566−1572.
(60) Nogami, M.; Hotta, S.; Kugimiya, K.; Matsubara, H. *J. Sol−Gel Sci. Technol.* **2010**, *56*, 107−113.
(61) Mahadik, S. A.; Kavale, M. S.; Mukherjee, S. K.; Rao, A. V. *Appl. Surf. Sci.* **2010**, *257*, 333−339.
(62) Abboud, J.-L. M.; Notari, R. *Pure Appl. Chem.* **1999**, *71*, 645−718.
(63) Graffion, J.; Cattoën, X.; Wong Chi Man, M.; Fernandes, V. R.; André, P. S.; Ferreira, R. A. S.; Carlos, L. D. *Chem. Mater.* **2011**, *23*, 4773−4782.
(64) Chaker, J. A.; Santilli, C. V.; Pulcinelli, S. H.; Dahmouche, K.; Briois, V.; Judeinstein, P. *J. Mater. Chem.* **2007**, *17*, 744−757.
(65) Benyahya, S.; Monnier, F.; Taillefer, M.; Man, M. W. C.; Bied, C.; Ouazzani, F. *Adv. Synth. Catal.* **2008**, *350*, 2205−2208.
(66) Molina, E. F.; Pulcinelli, S. H.; Santilli, C. V.; Briois, V. *J. Phys. Chem. B* **2012**, *116*, 7931−7939.
(67) Blanc, S.; Pigot, T.; Cugnet, C.; Brown, R.; Lacombe, S. *Phys. Chem. Chem. Phys.* **2010**, *12*, 11280−11290.
(68) Mills, A.; Hazafy, D.; Parkinson, J.; Tuttle, T.; Hutchings, M. G. *Dyes Pigmen.* **2011**, *88*, 149−155.
(69) Ronzani, F.; Trivella, A.; Arzoumanian, E.; Blanc, S.; Sarakha, M.; Richard, C.; Oliveros, E.; Lacombe, S. *Photochem. Photobiol. Sci.* **2013**, *12*, 1260−2169.
(70) Dunn, D. A.; Lin, V. H.; Kochevar, I. E. *Photochem. Photobiol.* **1991**, *53*, 47−56.
(71) Flors, C.; Nonell, S. *J. Photochem. Photobiol. A: Chem.* **2004**, *163*, 9−12.
(72) Manring, L. E.; Gu, C. L.; Foote, C. S. *J. Phys. Chem.* **1983**, *87*, 40−44.
(73) Olea, A. F.; Worrall, D. R.; Wilkinson, F.; Williams, S. L.; Abdel-Shafi, A. A. *Phys. Chem. Chem. Phys.* **2002**, *4*, 161−167.
(74) Murasecco-Suardi, P.; Gassmann, E.; Braun, A. M.; Oliveros, E. *Helv. Chim. Acta* **1987**, *70*, 1760−1773.
(75) Grajcar, L.; Ivanoff, N.; Delouis, J. F.; Faure, J. *J. Chim. Phys.* **1984**, *81*, 33−38.
(76) Ketsle, G. A.; Levshin, L. V.; Sokolova, L. K. *Opt. Spectrosc.* **1979**, *47*, 494−497.

(77) Shimizu, O.; Watanabe, J.; Naito, S.; Shibata, Y. *J. Phys. Chem. A* **2006**, *110*, 1735−1739.
(78) Kamat, P. V.; Lichtin, N. N. *J. Phys. Chem.* **1981**, *85*, 3864−3868.
(79) Oliveros, E.; Suardi-Murasecco, P.; Aminian-Saghafi, T.; Braun, A. M.; Hansen, H.-J. *Helv. Chim. Acta* **1991**, *74*, 79−90.
(80) Ragàs, X.; He, X.; Agut, M.; Roxo-Rosa, M.; Gonsalves, A.; Serra, A.; Nonell, S. *Molecules* **2013**, *18*, 2712−2725.
(81) Cantau, C.; Pigot, T.; Manoj, N.; Oliveros, E.; Lacombe, S. *ChemPhysChem* **2007**, *8*, 2344−2353.
(82) Arnbjerg, J.; Paterson, M. J.; Nielsen, C. B.; Jørgensen, M.; Christiansen, O.; Ogilby, P. R. *J. Phys. Chem. A* **2007**, *111*, 5756−5767.
(83) Scurlock, R. D.; Nonell, S.; Braslavsky, S. E.; Ogilby, P. R. *J. Phys. Chem.* **1995**, *99*, 3521−3526.
(84) Braun, A. M.; Maurette, M. T.; Oliveros, E. *Photochemical technology*; Wiley-VCH: Weinheim, 1991.
(85) Braslavsky, S. E. *Pure Appl. Chem.* **2007**, *79*, 293−465.
(86) Rodgers, M. A. J. *J. Am. Chem. Soc.* **1983**, *105*, 6201−6205.
(87) Bourdelande, J. L.; Karzazi, M.; Dicelio, L. E.; Litter, M. I.; Marqués Tura, G.; San Román, E.; Vinent, V. *J. Photochem. Photobiol. A: Chem.* **1997**, *108*, 273−282.
(88) Mosinger, J.; Lang, K.; Hostomský, J.; Franc, J.; Sykora, J.; Hof, M.; Kubat, P. *J. Phys. Chem. B* **2010**, *114*, 15773−15779.
(89) Jockusch, S.; Sivaguru, J.; Turro, N. J.; Ramamurthy, V. *Photochem. Photobiol. Sci.* **2005**, *4*, 403−405.
(90) Soggiu, N.; Cardy, H.; Habib Jiwan, J. L.; Leray, I.; Soumillion, J. P.; Lacombe, S. *J. Photochem. Photobiol. Chem.* **1999**, *124*, 1−8.
(91) Clennan, E. L. *Acc. Chem. Res.* **2001**, *34*, 875−884.
(92) Lacombe, S.; Cardy, H.; Simon, M.; Khoukh, A.; Soumillion, J. P.; Ayadim, M. *Photochem. Photobiol. Sci.* **2002**, *1*, 347−354.
(93) Schweitzer, C.; Schmidt, R. *Chem. Rev.* **2003**, *103*, 1685−1758.
(94) García-Rodríguez, F.; Pérez-Robles, F.; Manzano-Ramírez, A.; Vorobiev, Y.; González-Hernández, J. *Solid State Commun.* **1999**, *111*, 717−721.